International Journal of Hydrogen Energy 222 (2026) 154256

Contents lists available at ScienceDirect

International Journal of Hydrogen Energy

journal homepage: www.elsevier.com/locate/he

Energy management in offshore islanded hydrogen DC microgrids: A cost and electrolyzer efficiency optimization approach

Bawantha Indrajith [a,e,*], Kosala Gunawardane [a], Md Alamgir Hossain [b,e], Li Li [a], Robert Nicholson [c], Ramon Zamora [d], Mark Anthony Preece [f]

[a] School of Electrical and Data Engineering, Faculty of Engineering and IT, University of Technology Sydney, Sydney, NSW, 2007, Australia
[b] School of Engineering, University of Southern Queensland, Toowoomba, QLD, 4350, Australia
[c] Pitt & Sherry, Sydney, NSW, 2060, Australia
[d] School of Engineering, Computer and Mathematical Sciences, Auckland University of Technology, Auckland, 1010, New Zealand
[e] Blue Economy Cooperative Research Centre, Launceston, TAS, 7248, Australia
[f] The New Zealand King Salmon Company Ltd, Nelson, 7011, New Zealand

ARTICLE INFO

Handling Editor: Dr M Djukic

Keywords:
Offshore DC microgrid
Renewable energy
PEM electrolyzer
PEM fuel cell
Hydrogen storage
Energy management

ABSTRACT

In the real-time energy management of offshore islanded microgrids, determining the optimal operating points of storage systems, particularly in hydrogen-based storage, poses significant challenges. These arise from the stochastic nature of offshore Renewable Energy Sources (RES), variable power demand, and the volatility of hydrogen systems. To address these, a novel objective function has been developed that integrates electrolyzer system efficiency into the Energy Management Strategy (EMS) of a DC microgrid. Unlike most existing literature, which considers electrolyzer efficiency as a constant, this work treats efficiency as a dynamic variable that depends on operating current, temperature, and pressure. The behavior of the electrolyzer efficiency with respect to these parameters is modeled, verified, and subsequently incorporated into the EMS. A MINLP based EMS is developed to implement the proposed formulation, and its effectiveness is validated by demonstrating optimal microgrid performance under the above scenario. Notably, the impact of optimal temperature and pressure control is evidenced by electrolyzer efficiency improvements of 1.7% and 3.1% in the efficiency-focused and multi-objective scenarios, respectively. The proposed EMS is evaluated against a rule-based and heuristic (PSO) methods. In the cost-based case, the developed method shows 36.5% and 0.04% cost reductions relative to the rule-based approaches, and a 0.39% reduction relative to PSO. In the efficiency-based scheme, it attains 0.10% efficiency gain over PSO for the optimal temperature-pressure method, and in the multi-objective case, it delivers 7.40% efficiency gain versus PSO.

1. Introduction

Renewable energy is receiving increased attention worldwide due to global warming and climate change targets. Wind, solar photovoltaic (PV), wave, and tidal are among the most promising RES, each characterized by inherently intermittent power generation under varying weather conditions [1]. Simultaneously, hydrogen energy is also receiving the highest attention of all time from both academic and industrial perspectives [2]. The zero-carbon operations of electricity-to-storage and storage-to-electricity processes are the main reasons for this growing attention. Randomly integrating RES and hydrogen-based components can create issues in the control, operation, and management of traditional power grids [3]. As a promising alternative, microgrids integrate distributed generation, energy storage, and control systems, enabling flexible operation in both islanded and grid-connected configurations [4]. However, in applications such as small islands, isolated ships/aircraft, and offshore farms, connecting to the main grid poses challenges due to high costs and difficult geographic conditions. In such scenarios, microgrids often operate in islanded mode supported by sufficient energy storage technologies [5]. DC microgrids

* Corresponding author. School of Electrical and Data Engineering, Faculty of Engineering and IT, University of Technology Sydney, Sydney, NSW, 2007, Australia.
E-mail address: bawantha.polgollemudiyanselage@student.uts.edu.au (B. Indrajith).

https://doi.org/10.1016/j.ijhydene.2026.154256
Received 13 August 2025; Received in revised form 9 January 2026; Accepted 25 February 2026
Available online 4 March 2026

Nomenclature

EMS	Energy Management System	$\eta_{dc/dc}$	DC-DC convertor efficiency	w	Weight coefficient
PV	Photovoltaic	V_{cell}	Fuel-cell cell voltage	S_{B_min}	Minimum battery energy
ESS	Energy Storage Systems	J_{EL}	Electrolyzer current density	S_{B_max}	Maximum battery energy
RES	Renewable Energy Sources	P_{EL}^{rated}	Electrolyzer rated power	P_{Bd_min}	Minimum battery power
SOC	State of Charge	$v_{h\_EL}^{rated}$	Electrolyzer rated flow rate	P_{Bc_max}	Maximum battery power
FLC	Fuzzy Logic Control	d	Hydrogen density	P_{FC_mim}	Minimum fuel cell power
PLC	Programmable Logic Control	α	Coefficient of conversion	P_{FC_max}	Maximum fuel cell power
LA	Lead Acid	β	Coefficient of conversion	S_{H_min}	Minimum hydrogen level
LCOE	Levelized Cost of Energy	v_{h_EL}	Electrolyzer flow rate	S_{H_max}	Maximum hydrogen level
V2G	Vehicle to Grid	P_{FC}^{rated}	Fuel-cell rated power	P_{EL_min}	Minimum electrolyzer power
EV	Electric Vehicles	$v_{h\_FC}^{rated}$	Fuel-cell rated flow rate	P_{EL_max}	Maximum electrolyzer power
TPO	Temperature-Pressure Optimization	O_{cost}	Cost objective	T_{EL}	Electrolyzer operating temperature
MO	Multi Objective	C_{PV}	PV cost	T_{EL_mim}	Minimum electrolyzer temperature
PSO	Particle Swarm Optimization	C_W	Wind cos	T_{EL_max}	Maximum electrolyzer temperature
P_{PV}	PV power	C_{FC}	Fuel cell cost	P_{EL}^{H2}	Hydrogen pressure
η_s	PV overall efficiency	C_{EL}	Electrolyzer cost	$P_{EL\_min}^{H2}$	Minimum electrolyzer pressure
A	PV area	C_B	Battery cost	$P_{EL\_max}^{H2}$	Maximum electrolyzer pressure
γ	Temperature coefficient	T	Total operating power	ΔH_{LHV}	heat of combustion of hydrogen
t_0	Outside air temperature	n_{pv}	Number of PV panels	F	Faraday coefficient
I_r	Solar Irradiation	n_w	Number of wind generators	R	Universal gas constant
P_W	Wind Power	n_{fc}	Number of fuel cells	T_{cell}	Cell temperature
v	Current wind velocity	n_{el}	Number of electrolyzers	P_{EL}^{O2}	Oxygen Pressure
v_r	Rated wind velocity	n_b	Number of batteries	P_O	Standard pressure
v_{ci}	Cui-in wind velocity	$G_{PV,i}$	PV cost coefficient	α	Charge transfer coefficient
v_{co}	Cut-out wind velocity	$G_{W,j}$	Wind cost coefficient	Z	Number of transferred electrones
P_{Wr}	Rated wind power	$e_{FC,k}$	Fuel cell cost coefficients	j_0	Exchange current density
S_B	Battery energy level	$\eta_{FC,k}$	Fuel cell efficiency	P_{H2O}	Partial pressure of water vapor
Δt	Time interval	$e_{EL,n}$	Electrolyzer cost coefficient	ΔH_{vap}	Enthalpy of vaporization
P_B	Battery power	$\eta_{FC,n}$	Electrolyzer efficiency	d^m	Membrane thickness
η_c	Battery charging efficiency	$e_{B,m}$	Battery cost coefficient	δ^m	Swelling of the membrane
η_d	Battery discharging efficiency	η_{H2}^P	Hydrogen production efficiency	σ^m	Membrane conductivity
P_{FC}	Fuel-cell power	η_{H2}^F	Faraday efficiency	r_0	Resistances of the electrodes
V_{FC}	Fuel-cell voltage	η_{H2}^C	Compression efficiency	a_x	Fitting constant
I_{FC}	Fuel-cell current	η_{EL}	Electrolyzer efficiency	A_{el}	Active electrode area
P_{EL}	Electrolyzer power	O_{eff}	Efficiency objective	V_{cell}	Electrolyzer cell voltage
V_{EL}	Electrolyzer voltage	O_n	Normalized objective	N_{cell}	Number of cells
I_{EL}	Electrolyzer current	O_{costn}	Normalized cost objective	P_{EL_stack}	Electrolyzer stack voltage
S_H	Hydrogen storage level	O_{effn}	Normalized efficiency objective	P_{H2}^T	Temperature-dependent permeability

are particularly preferred because they offer higher efficiency, simpler control, and improved compatibility with renewable energy sources and storage systems [6].

In such microgrids, the energy management unit is responsible for the stable operation of the microgrid, intensively utilizing Energy Storage Systems (ESS) to store and dispatch energy with intermittent RES [7]. Energy is stored at ESS during energy surplus instances, and available energy at ESS is delivered to the microgrid during energy deficit instances. Without grid power, the only consideration is selecting storage strategies, such as battery and hydrogen storage. Generally, this selection is carried out considering cost-related procedures where low-cost operation is prioritized [8]. To properly control energy storage with reduced cost of operations, the formulation of the storage system cost and efficiencies needs to be carefully analyzed. This involves determining the most economical and efficient operating point of an islanded system, including intermittent RES, such as PV and wind, a battery storage system, and a hydrogen storage system, while satisfying complicated constraints related to each component [9].

The if-else rule-based strategy is a conventional method of energy management, in which a fixed number of scenarios that consider sets of rules and limits are developed. This strategy considers the available power deficit/surplus, the State of Charge (SOC) of storage units, and operational constraints to determine the system's operating point. However, failure to operate at an optimal point can lead to unnecessary charging or discharging of storage units, reduced component lifespan, increased operational costs, and decreased overall microgrid efficiency. To effectively utilize the optimal operating point in microgrid operation, many optimization strategies, including linear programming [10], dynamic programming [11], Fuzzy Logic Control (FLC) [12–14], stochastic and robust controlling [15–17] have been developed in the literature. In Ref. [18], a decentralized EMS is proposed for a DC microgrid that includes hydrogen storage, an electrolyzer, and a battery system. The proposed EMS strategy delivers better parallel operation of hydrogen and battery storage than conventional EMS strategies by keeping the SOC levels of both systems within linear operation. However, this strategy cannot achieve optimal solutions in system. A hybrid FLC and Programmable Logic Control (PLC) approach is developed in Ref. [12] to examine the impact of demand response and hydrogen systems, including an electrolyzer, hydrogen storage, and a fuel cell. Compared to cases involving only hydrogen systems, this configuration shows a significant reduction in charging and discharging costs for hydrogen storage. In Ref. [19], an islanded microgrid powered by RES, battery, and hydrogen is studied to optimize the energy storage arrangement of LI and LA batteries, PEM, and alkaline electrolyzer. Integrating alkaline electrolysis into the system has a lower cost compared to PEM electrolysis, and the integration of any type of electrolysis significantly reduces the Levelized Cost of Energy (LCOE). Furthermore, the effect of temperature on electrolyzer and fuel cell systems is considered. However, EMS is designed to achieve the LCOE by considering only one temperature point for electrolyzer and fuel cell systems. In Ref. [20], an EMS strategy is proposed for energy management in a hydrogen-based DC microgrid consisting of PV, fuel cells, electrolyzer, hydrogen storage, V2G EV stations, and battery storage. Results for different RES conditions indicate that the proposed EMS strategy can reduce the number of times hydrogen-related devices are switched on/off, while effectively utilizing the V2G station with the microgrid as an energy storage system.

In [12], a combination of a hydrogen energy system and demand

response is analyzed through four different case studies to evaluate their impact on the EMS. However, this study does not discuss the EMS strategy in detail and focuses solely on the microgrid's operating costs. Moreover, the modeling of the hydrogen system is not considered comprehensively. In Ref. [21], a novel EMS is developed to improve the smooth transition between hydrogen and electrical systems. Specifically, the microgrid's net load power is split into low- and high-frequency components, with the low-frequency component assigned to the hydrogen system and the high-frequency component assigned to the electrical system. Although priority is given to the hydrogen system, the objectives neglect the efficiency of the hydrogen components in the formulation. In Ref. [22], a hydrogen-based microgrid is developed to minimize hydrogen consumption. An equivalent consumption minimization strategy is used in the objective; however, the electrolyzer's impact is not accounted for in the formulation. In Ref. [23], an interesting study was conducted on hydrogen production using offshore wind energy. The nonlinear hydrogen production efficiency of the electrolyzer system is considered in the microgrid EMS, and the results indicate that the operating cost can be reduced by accounting for the nonlinear efficiency, particularly under offshore wind profiles. However, this study considers only constant operating environments. In Ref. [24], a two-stage scheduling approach is developed, combining day-ahead and real-time strategies, which results in reduced operational costs and environmental impacts. Specifically, the impact of the diesel generator is significantly reduced through the integration of the hydrogen system; however, only general cost terms are considered in the objective formulation. In Ref. [25], a DC-link-based voltage control strategy is developed for an off-grid DC microgrid integrated with hydrogen systems. Stable operation is achieved, including in the system's hardware implementation. However, aspects such as cost and hydrogen system efficiency are not considered in this study.

In most of the literature reported above, the focus lies in algorithmic improvements and the use of economic or environmental objectives, with limited attention to the efficiency-oriented control of hydrogen systems. Electrolyzer efficiency, in particular, is often assumed to be constant, despite its dependence on key operational variables such as current density, temperature, humidity, and pressure. This simplification can lead to inefficient operations, especially in offshore and islanded scenarios with diverse environmental conditions, where energy storage systems, such as hydrogen storage, significantly impact overall system performance. Moreover, little consideration is given to the sensitivity of electrolyzer performance to temperature and pressure changes, which are crucial for accurate modeling and real-world implementation. To address these gaps, the major contributions of this work are as follows:

- A novel optimization formulation integrating electrolyzer system efficiency is developed to optimize hydrogen system utilization in an offshore islanded DC microgrid.
- Electrolyzer system efficiency is dynamically modeled as a function of operating current, temperature, and pressure, and integrated into the EMS.
- A multi-objective optimization framework is proposed, offering adaptability to operator requirements for both cost-effective and efficient microgrid management.
- The impact of electrolyzer operating pressure and temperature sensitivity on the microgrid EMS is examined using the proposed approach.
- The proposed EMS is compared with a rule-based and a meta-heuristic EMS to validate its effectiveness for offshore hydrogen-based DC microgrids.

The structure of this paper is as follows. Section 2 provides an overview of offshore hydrogen-based DC microgrids. Section 3 presents detailed descriptions of microgrid components. Section 4 focuses on modeling the electrolyzer system efficiency and configuring the stack. In Section 5, the formulation of the optimization problem for the EMS is developed. Section 6 presents the simulation results for five distinct case studies. Section 7 compares the performance of the proposed EMS against three alternative EMS, providing validation of the developed method. Finally, Section 8 concludes the study.

2. Offshore hydrogen-based DC microgrid

A hydrogen-integrated islanded DC microgrid, operated with RES to meet an offshore fish farm load demand, is illustrated in Fig. 1. Microgrid consists of five solar generators (6 kW/gen) and four wind generators (5 kW/gen) to meet the load demand, typical of an offshore salmon farm, such as The New Zealand King Salmon Company's Blue Endeavour farm. In addition, a microgrid consists of two types of energy storage, battery and hydrogen. The battery storage has three individual Li-ion battery units. Hydrogen energy storage has three main sections: the electrolyzer unit, the hydrogen storage unit, and the fuel cell unit. Electrolyzers use microgrid renewable energy from PV and wind to generate hydrogen and store it in the hydrogen storage. Fuel cells use the stored hydrogen to supply power back to the microgrid DC bus.

Determining the optimal sizes of microgrid parameters falls outside the scope of this research. Therefore, the system specifications were selected as the best applicable scenarios as shown in Table 1. The EMS manages energy to ensure the requirements of load power demand over 48 h in 1-h intervals, operating battery and hydrogen energy storage. Generally, battery capacity is estimated to be three times greater than the maximum load demand to maintain a continuous supply for at least 3 h. The battery capacity is selected to supply the local load for 3 h, as required due to the unexplored nature of hydrogen systems and stochastic RES. The operation of all RES in this study is based on the maximum power point to achieve optimal power extraction. Therefore, managing battery and hydrogen energy storage becomes critical.

3. System modelling

3.1. Solar PV

In a solar panel, sunlight is converted into DC electricity by utilizing PV cells. PV generators are operated in MPPT mode to utilize the maximum energy produced. Solar irradiation data for Cape Grim, Tasmania, Australia, were obtained from the Australian Bureau of Meteorology [26]. One-minute global horizontal irradiance and ambient temperature data were processed to obtain hourly average values for the period from January to March. The PV Power output, P_{PV}, is modeled using the equation below,

$$P_{PV} = \eta_s * A * I_r * (1 + \gamma(t_0 - 25)) \quad (1)$$

where η_s and A are the overall efficiency and the area of the PV panels, respectively. I_r, t_0 and γ denote the solar irradiation, outside air temperature (28 °C), and the temperature coefficient of maximum output

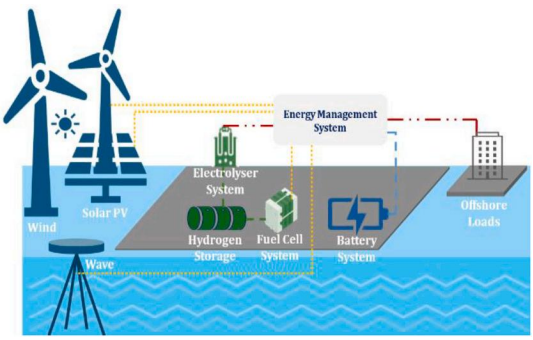

Fig. 1. Islanded hydrogen-based DC microgrid system.

Table 1
Input parameters of the islanded hydrogen-based DC microgrid.

Parameter	Value	Unit
PV generators		
Area, A	125	m^2
Efficiency, η_s	16	%
Power, P_{PV}	30	kW
Wind generators		
Cut-in velocity, v_{ci}	3	ms^{-1}
Cut-out velocity, v_{co}	25	ms^{-1}
Rated velocity, v_r	10	ms^{-1}
Power, P_W	20	kW
Hydrogen storage		
Initial storage level, $S_{H,0}$	300	L
Minimum storage level, S_{H_min}	100	L
Maximum storage level, S_{H_max}	600	L
Battery storages		
Initial energy level, $S_{B,0}$	100	kWh
Maximum energy level, S_{B_min}	200	kWh
Minimum energy level, S_{B_max}	50	kWh
Energy capacity	200	kWh
Maximum charging rate, P_{Bc_max}	50	kW
Maximum discharging rate, P_{Bd_max}	−50	kW
Fuel cell system		
Minimum operating power, P_{FC_min}	10	kW
Maximum operating power, P_{FC_max}	30	kW
Electrolyzer system		
Minimum operating power, P_{EL_min}	5	kW
Maximum operating power, P_{EL_max}	50	kW

power ($-0.005\ ^0C^{-1}$) [27].

3.2. Wind generation

$$P_W = \begin{cases} 0 \quad ; if\ v < v_{ci}\ or\ v > v_{co} \\ P_{Wr} * \dfrac{v^3 - v_{ci}^3}{v_r^3 - v_{ci}^3} : if\ v_{ci} \le v \le v_r \\ P_{Wr} : if\ v_r < v \le v_{co} \end{cases} \quad (2)$$

In wind generators, the kinetic energy of wind is converted into electrical energy based on aerodynamic principles. The wind turbine is mounted at a specific height, where the wind hits the turbine blades, initiating the turbine's rotation. Wind speed measurements at 150 m height from the Tasmanian Earth Resources Satellite Station facility on Droughty Hill, Tasmania, Australia, were obtained from the CSIRO Data Access Portal [28]. The 10-min average wind speed records were further processed to generate hourly mean values for use in the proposed model. Power output, P_W , is modeled using the below piece-wise relationship. v, v_r, v_{ci} and v_{co} represent current, rated, cut-in, and cut-out wind speeds, P_{Wr} stands for rated electrical power output [29].

3.3. Battery storage system

Rechargeable Lithium-Ion battery storage units can either charge or discharge energy based on the available net power of the microgrid and associated costs. The charging and discharging modes of the battery are modeled as follows.

$$S_B(t) = S_B(t-1) + \Delta t P_B(t)\eta_c;\ \text{at charging}\ (P_B(t) > 0) \quad (3)$$

$$S_B(t) = S_B(t-1) + \frac{\Delta t P_B(t)}{\eta_d};\ \text{at discharging}\ (P_B(t) < 0) \quad (4)$$

$S_B(t)$ and Δt denotes the battery energy level and the time interval (1h). P_B, η_c and η_d represent the charging/discharging power, charging efficiency (98%), and discharging efficiency (98%).

3.4. PEM fuel cell system

A PEM fuel cell converts the chemical energy of the fuel into electrical energy through an electrochemical process. The core of a PEM fuel cell consists of two electrodes separated by a proton exchange membrane. The membrane only allows protons to pass through while blocking electrons [30,31]. The process starts when hydrogen gas is introduced to the anode side of the fuel cell, where a catalyst splits the hydrogen molecules into protons and electrons. Protons pass through the proton exchange membrane to the cathode, while electrons travel through an external circuit, generating an electric current. On the cathode side, oxygen from the air combines with the protons and electrons to produce water and heat. The generated PEM fuel cell stack power, P_{FC}, is expressed as,

$$P_{FC} = V_{FC} * I_{FC} \quad (5)$$

where V_{FC}, I_{FC} represent the stack voltage and current [32].

3.5. PEM electrolyzer system

A PEM electrolyzer uses electricity to split water into oxygen and hydrogen. Water is fed to the anode side, where it splits the water molecules into protons, electrons, and oxygen. The protons pass through the membrane to the cathode, while the electrons flow through an external circuit. On the cathode side, the protons combine with electrons to form hydrogen [33]. A PEM electrolyzer stack is developed by combining several PEM electrolyzer cells. The PEM electrolyzer stack power consumption, P_{EL}, can be expressed as follows,

$$P_{EL} = V_{EL} * I_{EL} \quad (6)$$

where V_{EL} and I_{EL} denote the electrolyzer stack operating voltage and electrolyzer operating current [34].

3.6. Hydrogen storage

Liquid hydrogen offers a higher energy density per unit volume, resulting in a comparatively lower weight [35]. In this study, the produced hydrogen from the PEM electrolyzer system is converted to storable liquid conditions, and then, liquid hydrogen is converted to gaseous hydrogen suitable for fuel cell operation [36]. Therefore, the state of charge of hydrogen energy storage (S_H) is modeled as follows,

$$S_H(t+1) = S_H(t) + [\, n_{EL} * \alpha * P_{EL}(t)\,]\Delta t - \left[\, \frac{1}{n_{FC}} * \beta * P_{FC}(t) \right] \Delta t \quad (7)$$

where S_H represents the hydrogen storage level, P_{EL} and P_{FC} represent the operating power of the PEM electrolyzer and PEM fuel cell. Also, α, n_{EL}, β and n_{FC} denotes coefficients of conversion for electrolyzer power to a hydrogen flow, electrolyzer system efficiency, coefficients of conversion for fuel cell power to the required hydrogen flow, and fuel cell system efficiency, respectively. In this study, the energy required to convert hydrogen gas into H_2 liquid and vice versa is not taken into account. Additionally, assuming a constant hydrogen flow from the electrolyzer to storage and then to the fuel cell, the relationships between electrolyzer power and hydrogen generation rate, as well as between fuel cell hydrogen consumption rate and power output, are assumed to be linear.

Assuming the hydrogen production rate of electrolyzer (v_{h_EL}) is proportional to the electrolyzer operating power (P_{EL}), the hydrogen production mass rate (kg/h), at a given electrolyzer operating power can be calculated as (8), (9),

$$\frac{P_{EL}^{rated}}{P_{EL}} = \frac{v_{h\_EL}^{rated}}{v_{h\_EL}} \quad (8)$$

$$v_{h\_EL} = v_{h\_EL}^{rated} * \frac{P_{EL}}{P_{EL}^{rated}} \tag{9}$$

If the loss is negligible in the liquification process, it can be assumed that the liquid hydrogen has the same hydrogen production rate (kg/h). So, the hydrogen density (d) is used in (10) to convert it to a volumetric rate (m^3/h). Equation (11) is an arrangement of (10).

$$v_{h\_EL} = P_{EL} * \frac{v_{h\_EL}^{rated}}{P_{EL}^{rated}} * \frac{1}{d} \tag{10}$$

$$v_{h\_EL} = P_{EL} * \left(\frac{v_{h\_EL}^{rated}}{P_{EL}^{rated} * d} \right) \tag{11}$$

Coefficient α can be derived using the rated hydrogen flow rate, the rated electrolyzer power, and the hydrogen density. Similarly, the coefficient β can be derived for fuel cells as well.

$$\alpha = \left(\frac{v_{h\_EL}^{rated}}{P_{EL}^{rated} * d} \right) \tag{12}$$

$$\beta = \left(\frac{v_{h\_FC}^{rated}}{P_{FC}^{rated} * d} \right) \tag{13}$$

3.7. Power electronic converters

Power electronic converters (DC-DC,DC-AC) are modeled to operate at a constant efficiency. DC-DC converters are assumed to be operated at 95%, while DC-AC converters are assumed to be operated at 90% based on the typical efficiencies in these converters.

3.8. Offshore load profile

This study utilizes measured load data from The New Zealand King Salmon Company's aquaculture facility, representing the operational power demand. A 48-h period was selected for analysis, using hourly maximum load values derived from the load data recorded between January to March of 2024. The load profile peaks at 38 kW, representing typical operational conditions for the study. The dataset was obtained under an industry collaboration agreement and is therefore not publicly available (see Fig. 2).

4. Electrolyzer system efficiency modeling

The PEM electrolyzer's single-cell efficiency behavior model presented in Refs. [37,38] has been studied as the baseline in this study. Electrolyzer system efficiency consists of three elements, namely hydrogen production efficiency, $\eta_{H_2}^{p}$, Faraday's efficiency, $\eta_{H_2}^{F}$, and compression efficiency, $\eta_{H_2}^{C}$. $\eta_{H_2}^{p}$ primarily relates to the electrochemical reaction stage, where it measures the ratio of the actual hydrogen energy output to the total electrical energy input, as illustrated in (14). $\eta_{H_2}^{F}$ accounts for hydrogen loss due to permeation as in (15). Hydrogen permeation results in a direct loss of storable energy, whereas oxygen permeation contributes to water formation [37,39]. Compression efficiency becomes relevant after hydrogen production, as hydrogen must be compressed for storage or transportation. In this study, $\eta_{H_2}^{C}$ is selected to be constant at 95% throughout the operation, as illustrated in 16. The overall efficiency, η_{EL}, is the multiplication of hydrogen production, Faraday, and compression efficiencies, given in (17). It is a function of current density, temperature, and partial pressures of oxygen and hydrogen. Parameters of the developed EMS are given in Table 3 [37, 38].

$$\eta_{H_2}^{p} = \left(\frac{1.25}{\left| 1.48 + \frac{P_{H2O}}{2F} \left(\frac{1}{p_{EL}^{H2}} + \frac{1}{2p_{EL}^{O2}} \right) \Delta H_{vap} - U_{cell} \right| + 1.229 - 0.9{*}10^{-3}(T_{cell} - 298) + \frac{RT_{cell}}{2F} ln\left(\frac{p_{EL}^{H2} * \sqrt{p_{EL}^{O2}}}{p_O \sqrt{p_O}} \right) + \frac{RT_{cell}}{\alpha zF} ln\left(\frac{j}{j_0} \right) + \left(r_0 + \frac{d^m \delta^m}{\sigma^m} \right) j} \right) \tag{14}$$

$$\eta_{H_2}^{F} = \left(1 - \frac{2\left(Fp_{H_2}^{T} \frac{p_{EL}^{H2} + p_{EL}^{O2}}{d^m \delta^m} + \frac{a_x}{d^m \delta^m} j \right)}{j} \right) \tag{15}$$

$$\eta_{H_2}^{C} = 95\% \tag{16}$$

$$\eta_{EL} = \eta_{H_2}^{p} * \eta_{H_2}^{F} * \eta_{H_2}^{C} \tag{17}$$

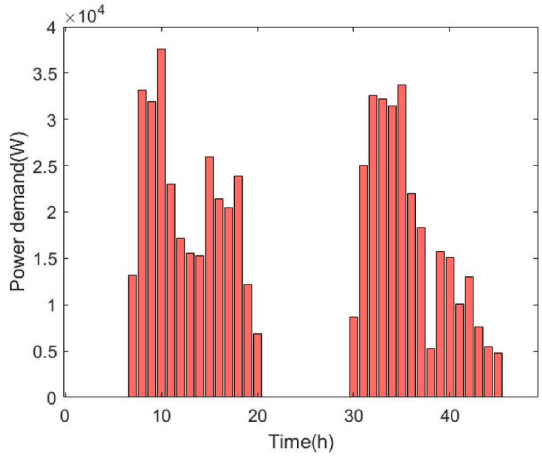

Fig. 2. Hourly maximum load profile.

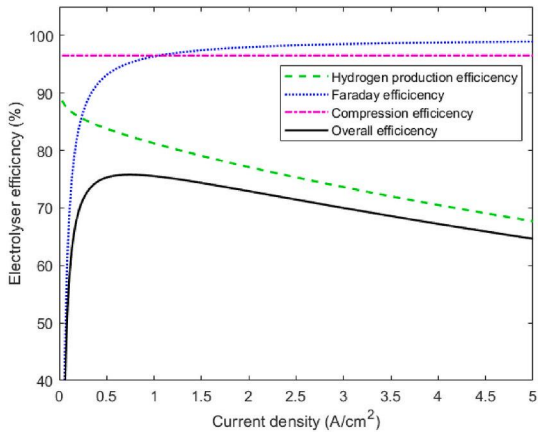

Fig. 3. Electrolyzer efficiency curves [32].

These models are then extended to investigate efficiency variations as a function of operating temperature, pressure, and stack performance. Fig. 3 shows how electrolyzer efficiency changes with current density, based on the discussion in Ref. [38], under fixed operating conditions of 10 bar and 350 K. Hydrogen production efficiency declines as the current density increases. In contrast, Faraday efficiency is low at lower current densities, rises nonlinearly to a peak, and then decreases slightly. Therefore, Faraday efficiency dominates the overall efficiency variation at lower current densities, while at higher current densities, hydrogen production efficiency becomes more significant.

Based on this, the electrolyzer's overall efficiency variations with both current density and operating pressure, at a constant operating temperature of 350 K, are constructed and illustrated in Fig. 4a. Once the operating pressure increases, the overall efficiency increases with current density initially. Then the overall efficiency decreases with both operating pressure and current density. Then the overall efficiency variation with both current density and operating temperature, at a constant operating pressure of 10 bar, is illustrated in Fig. 4b. Once the operating temperature increases, the overall efficiency varies in the same pattern as with current density. Finally, overall efficiency variations with both operating temperature and pressure, at constant current densities (1-5 A/cm^2), are illustrated in Fig. 4c. The overall efficiency varies nonlinearly with operating pressure, peaking around 4-10 bar. Once the temperature increases, the same behavior is lifted to higher efficiencies. Variation in the overall efficiency at lower pressures, at a constant current density, is more strongly influenced by pressure than by temperature. The overall efficiency pattern shifts downward by nearly 10% from 1 to 5 A/cm^2.

A typical PEM electrolyzer system, as illustrated in Fig. 5, consists of multiple PEM stacks, with each stack comprising several series-connected PEM cells to meet the required performance specifications [48]. In this study, the system includes a single stack containing 200 series-connected cells. The PEM electrolyzer system is designed to be powered by a 400 V DC bus of the microgrid via a DC-DC buck converter. Each cell operates at approximately 1.9 V, with a total stack voltage of 380 V DC. This configuration confirms that the 380 V stack is connected to the 400 V DC bus through a converter. Power, distributed to the electrolyzer, P_{EL}, is reduced due to power loss in the DC-DC converter as given in (18). Electrolyzer stack power is illustrated using electrolyzer stack voltage, V_{EL_stack}, and electrolyzer current, I_{EL}, as given in (19). An electrolyzer stack is a combination of electrolyzer cells. So, electrolyzer current is illustrated using electrolyzer stack power, P_{EL_stack}, electrolyzer cell voltage, V_{cell}, number of cells, N_{cell}, and converter efficiency, $\eta_{dc/dc}$, in (20) [49]. Electrolyzer current density, J_{EL}, is calculated using the stack operating current and active electrode area, A_{EL}, as illustrated in (22) and (23).

$$P_{EL}{}^{*}\eta_{dc/dc} = P_{EL\_stack} \tag{18}$$

$$P_{EL}{}^{*}\eta_{dc/dc} = V_{EL\_stack}{}^{*}I_{EL} \tag{19}$$

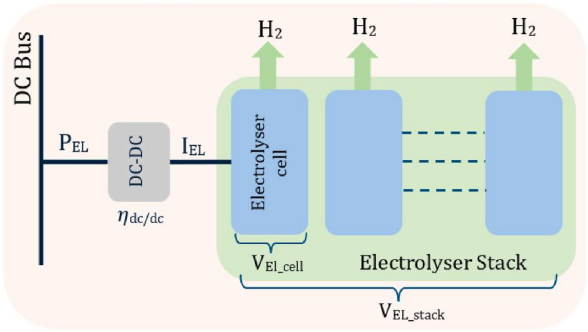

Fig. 5. Configuration of the PEM electrolyzer stack.

$$P_{EL}{}^{*}\eta_{dc/dc} = N_{cell}{}^{*}V_{cell}{}^{*}I_{EL} \tag{20}$$

$$I_{EL} = \frac{P_{EL}{}^{*}\eta_{dc/dc}}{N_{cell}{}^{*}V_{cell}} \tag{21}$$

$$J_{EL} = \frac{I_{EL}}{A_{EL}} \tag{22}$$

$$J_{EL} = \frac{P_{EL}{}^{*}\eta_{dc/dc}}{N_{cell}{}^{*}V_{cell}{}^{*}A_{EL}} \tag{23}$$

5. The proposed objective function formulations

5.1. Cost function formulation

The total cost of the DC microgrid is illustrated as O_{cost} in (24), and t represents the time instant. $C_{PV,i}$, $C_{W,j}$, $C_{FC,k}$, $C_{EL,n}$, and $C_{B,m}$ denote the cost terms of solar PV, wind, fuel cell, electrolyzer systems and degradation cost of the battery system. Apart from that, n_{pv}, n_w, n_{fc}, n_{el}, n_b, and T represent the number of solar PV generators, wind generators, fuel cell units, electrolyzer units, battery storage units, and total operation time. A general cost model is introduced at this stage to emphasize the role of electrolyzer system efficiency in EMS, rather than conducting a detailed economic analysis, which is out of the scope of the study. For renewable energy sources, only marginal operation and maintenance costs are

Table 2
EMS input data [40–45].

Parameter	Value	Parameter	Value
G^E_{PV} ($/kWh)	0.01	α	4.28e-4
G^E_W ($/kWh)	0.01	β	3.62e-4
e_{EL} ($/kWh)	0.0375	n_{FC} (%)	0.6
e_{FL} ($/kWh)	0.0375	n_{EL} (%)	0.75
e_b ($/kWh)	0.0125		

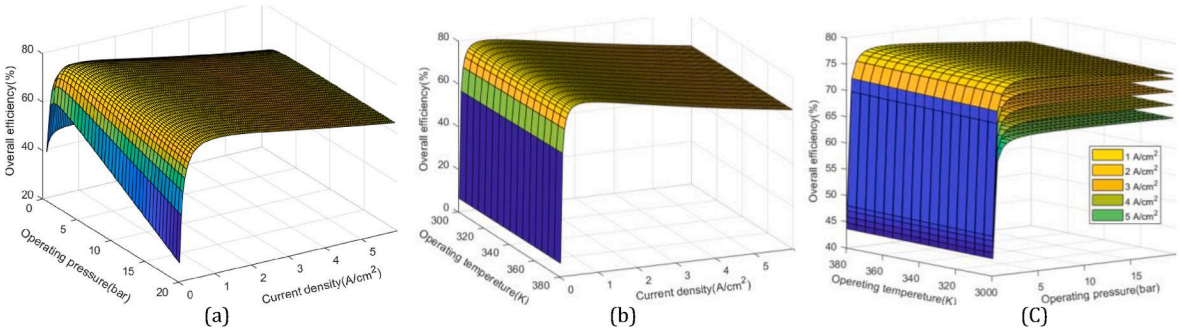

Fig. 4. Electrolyzer system's overall efficiency (a) with pressure and current density (b) with temperature and current density (C) with pressure and temperature.

Table 3
Parameters of PEM electrolyzer [37,38,46,47].

Parameter	Value	Parameter	Value
ΔH_{LHV} (kJ/mol)	241	d^m (μm)	51×10^{-4}
F (C/mol)	96500	δ^m	1.15
R (J/mol K)	8.314	σ^m (s/cm)	0.137
T_{cell} (K)	350	R_0 (mΩ/cm^2)	27×10^{-3}
P_O (bar)	4	$p^T_{H_2}$ (mol/cm s Pa)	5.31×10^{-16}
α	0.43	α_x (cm)	1.2×10^{-5}
z	2	$\eta^C_{H_2}$ (%)	0.95
j_0 (A/cm^2)	8×10^{-6}	A_{el} (A/cm^2)	25
P_{H2O} (Pa)	47948	V_{cell} (V)	1.9
ΔH_{vap} (kJ/mol)	41.572	N_{cell}	200

considered. The electrolyzer cost accounts for electrical energy consumption, while the fuel cell cost reflects efficiency losses and capital recovery expenditure. Battery degradation cost is based solely on cycle-induced degradation. This structure allows the EMS to remain focused on hydrogen dynamics while still addressing basic economic considerations. When selecting the coefficients in Table 2, the US Department of Energy hydrogen program record data [40,41], and several published data have been considered.

$$O_{cost} = \sum_{t=1}^{T} \left[\sum_{i=1}^{n_{pv}} C_{PV,i}(t) + \sum_{j=1}^{n_w} C_{W,j}(t) + \sum_{k=1}^{n_{fc}} C_{FC,k}(t) + \sum_{n=1}^{n_{el}} C_{EL,n}(t) + \sum_{m=1}^{n_b} C_{B,m}(t) \right] \tag{24}$$

The cost functions of a solar PV and a wind generation system are illustrated in (25) and (26), respectively, where $G^E_{PV,i}$ and $G^E_{W,j}$ denote the operation and maintenance cost per unit generated by the solar PV ($/kWh) and wind turbine ($/kWh).

$$C_{PV,i}(t) = G^E_{PV,i} * P_{PV,i}(t) * \Delta t \tag{25}$$

$$C_{W,j}(t) = G^E_{W,j} * P_{W,j}(t) * \Delta t \tag{26}$$

The cost function of the PEM fuel cell system is illustrated in (27), where $e_{FC,k}$ and $\eta_{FC,k}$ represent the cost coefficient ($/kWh) and efficiency of the PEM fuel cell.

$$C_{FC,k}(t) = \frac{e_{FC,k} * P_{FC,k}(t)}{\eta_{FC,k}} * \Delta t \tag{27}$$

The cost function of the PEM electrolyzer system is illustrated in (28), where $e_{EL,n}$ and $\eta_{FC,n}$ represent the cost coefficient ($/kWh) and efficiency of the PEM electrolyzer.

$$C_{EL,n}(t) = e_{EL,n} * P_{EL,n}(t) * \Delta t \tag{28}$$

The degradation cost of the battery system is expressed in (29), where $e_{B,m}$ and $P^d_{B,m}$ represent the degradation cost coefficient ($/kWh) and the discharging power of the battery system.

$$C_{B,m}(t) = e_{B,m} * P^d_{B,m}(t) * \Delta t \tag{29}$$

5.2. Electrolyzer system efficiency function formulation

Electrolyzer system efficiency consists of three elements, namely hydrogen production efficiency, $\eta^p_{H_2}$, Faraday's efficiency, $\eta^F_{H_2}$, and compression efficiency, $\eta^C_{H_2}$. Section 4 discusses the comprehensive modeling of the PEM electrolyzer system efficiency. The overall efficiency, η_{EL}, is the multiplication of hydrogen production, Faraday and compression efficiencies, given in (14), (15), (16) and (17). Using these formulations, the efficiency objective, O_{eff}, is formalized as follows.

$$O_{eff} = \sum\nolimits_{t=1}^{T} \eta_{EL}(t) \tag{30}$$

5.3. Multi-objective function formulation

Both the operating cost and the electrolyzer system efficiency are considered simultaneously in the objective formulation. As these two objectives consist of different units and scales, min–max normalization is applied to bring them onto a common range and ensure balanced contribution in the combined objective. Normalization is performed using the following expressions.

$$O_{cost_n} = \frac{O_{cost} - O^{min}_{cost}}{O^{max}_{cost} - O^{min}_{cost}} \tag{31}$$

$$O_{eff_n} = \frac{O_{eff} - O^{min}_{eff}}{O^{max}_{eff} - O^{min}_{eff}} \tag{32}$$

This maps both cost and efficiency values to the interval [0,1] individually, while eliminating biases caused by scale mismatches. With the normalized terms established, the final objective function is formulated as a weighted sum. Cost term is retained as a positive component to be minimized, while the efficiency term is subtracted to reflect its maximization within the same minimization framework. The resulting expression for the normalized combined objective is illustrated in (33), where O_n, $O_{cos\ t_n}$, O_{eff_n}, $w \in$[0.1,0.9] represents the final weighted normalized objective, normalized cost objective, normalized efficiency objective, and weight coefficient (0.1 steps from 0.1 to 0.9).

$$O_n = [(1-w) * O_{cos\ t_n}] - [w * O_{eff_n}] \tag{33}$$

Since both $O_{cos\ t_n}$ and O_{eff_n} are bounded between 0 and 1, and the weighting factor w lies within the range [0.1, 0.9], the resulting objective On is bounded within the interval $[-w, 1-w]$. This ensures that the final objective remains within a well-defined range, which, for all considered weights, falls approximately within [–1, 1].

5.4. Constraints

The optimization algorithm must satisfy the power balance of the microgrid as follows, where $P_B(t)$ and $P_L(t)$ represent the battery and load power levels.

$$P_{PV}(t) + P_W(t) + P_{FC}(t) - P_B(t) = P_L(t) + P_{EL} \tag{34}$$

Battery energy levels must satisfy the maximum and minimum allowable storage levels of the battery system.

$$S_{B\_min} \le S_B(t) \le S_{B\_max} \tag{35}$$

Charging and discharging power levels must satisfy the limitations of the battery system as follows.

$$P_{Bd\_max} \le P_B(t) \le P_{Bc\_max} \tag{36}$$

PEM fuel cell power must satisfy the following allowable power limitations.

$$P_{FC\_mim} \le P_{FC}(t) \le P_{FC\_max} \tag{37}$$

Hydrogen storage must maintain the allowable maximum and minimum levels of the storage state.

$$S_{H\_min} \le S_H(t) \le S_{H\_max} \tag{38}$$

The power levels of the PEM electrolyzer must also meet the allowable limits.

$$P_{EL\_min} \le P_{EL}(t) \le P_{EL\_max} \tag{39}$$

Two additional constraints related to hydrogen pressure (P^{H2}_{EL}) and operating temperature (T_{EL}) of the electrolyzer systems are used in specific case studies. They are allowed to vary within maximum and minimum levels, considering electrolyzer requirements and limitations.

$$T_{EL\_mim} \le T_{EL} \le T_{EL\_max} \tag{40}$$

$$P^{H2}_{EL\_mim} \leq P^{H2}_{EL} \leq P^{H2}_{EL\_max} \quad (41)$$

6. Case studies

The YALMIP toolbox for modeling and optimization in MATLAB has been used in this study [50]. BMIBNB solver, combined with the Gurobi optimizer, is used for solving the underlying Mixed-Integer Nonlinear Programming (MINLP) optimization problem [51]. Five case studies were conducted to evaluate the performance of the proposed novel EMS strategy. Fig. 6 presents the workflow of the developed EMS, along with the corresponding case study and validation phases.

6.1. Case 1: Cost optimization

The DC microgrid considered in this study is operated to achieve minimum cost operation over as O_{cost} in (24), subject to various constraints. Achieved optimal power schedule profiles, battery storage profile, and hydrogen storage profile of the minimum cost-based EMS strategy are given in Fig. 7a. At t = 0, the battery system begins charging, as the renewable energy generated by the wind system exceeds the load demand. Since the objective function considers only cost, the majority of excess renewable energy is managed by the battery storage system, except in critical cases. During such instances, when renewable generation is high and the battery is nearly fully charged, the electrolyzer system begins operating to utilize the remaining surplus energy. Fig. 7b represents the battery storage and hydrogen storage levels for 48h. Since the associated costs are high, the cost optimization strategy reduces the operation of electrolyzer and fuel cell systems. In this case, the total electricity cost for the microgrid operation is $191.69 for 48h.

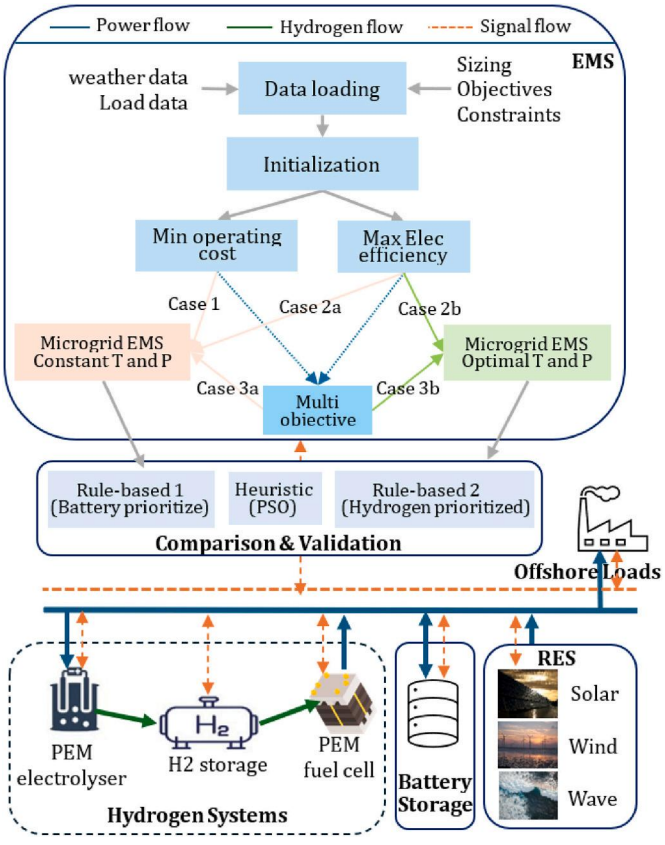

Fig. 6. Workflow of the developed microgrid EMS.

6.2. Case 2a: Optimization of PEM electrolyzer system efficiency

In this scenario, the DC microgrid is operated to achieve maximum efficiency operation of the PEM electrolyzer system. The combined efficiency of the PEM electrolyzer system can be expressed as O_{eff} in equation (30). Fig. 8a illustrates the optimized power allocations under the electrolyzer efficiency optimization scheme. With all relevant power and energy constraints satisfied, the results clearly demonstrate the effectiveness of the proposed objective function based on electrolyzer efficiency in achieving optimal microgrid operation. Significantly, this study introduces a nonlinear electrolyzer efficiency function as the sole objective, thereby replacing the conventional assumption of a constant efficiency. The formulated objective function indicates that the electrolyzer's operating power is directly linked to its current density, which in turn affects the system's efficiency. As a result, the electrolyzer tends to operate at higher power ratings, leading to more frequent operation of the fuel cell and battery systems. Since cost is not considered in this case, high utilization of the electrolyzer, fuel cell, and battery systems is observed, as in Fig. 8a.

Fig. 8b represents the storage levels of the battery and the hydrogen storage. Due to the continuous operation of the electrolyzer, the fuel cell also operates to maintain the energy balance. Although the electrolyzer and fuel cell operate at nearly the same power levels, the fuel cell consumes more hydrogen than is produced through electrolysis. This is primarily due to the higher heating value of hydrogen relative to its energy density, the inherently low efficiency of the fuel cell, and the presence of parasitic power losses. The battery supports the operation of both the electrolyzer and the fuel cell by charging and discharging as needed, thereby maintaining energy levels within acceptable limits. In this simulation, the electrolyzer system achieves a mean operational efficiency of 72.19% with a total microgrid operating cost of $986.1 over a 48-h time period.

6.3. Case 2b: Temperature and Pressure Optimized (TPO) PEM electrolyzer system efficiency

In Section 6.2, only the current density is allowed to vary to achieve maximum efficiency of the electrolyzer system. In this section, the operating temperature and pressure are also allowed to vary within predefined ranges, as described in Section 5.4. The operating temperature is allowed to vary between 310 K and 360 K, while the operating pressure can range from 1 bar to 20 bar. The optimization framework determines the optimal operating conditions that maximize the electrolyzer system efficiency, taking into account the hourly operating power of the electrolyzer. These operating regions are selected based on the overall efficiency modeling of the selected electrolyzer system, as described in Section 4. In this scenario, the EMS slightly regulates the temperature around 330 K, while the pressure varies between 9 bar and 11 bar. Notably, pressure indicates an inverse relationship with fuel cell power, fluctuating within this range as the power output changes. Fig. 9a represents the optimized power profiles, indicating that the operating power curves of both the electrolyzer and fuel cell are smoothed, with reduced fluctuations. Average operating power of the electrolyzer and fuel cells increased from 22.84 kW to 27.01 kW to 28.91 kW and 36.1 kW, respectively. However, the battery system operates similarly to the previous scenario in most cases, contributing to the microgrid's power balance. Both storage units store and dispatch energy in a manner similar to the previous case, as illustrated in Fig. 9b. In this scenario, the electrolyzer system achieves a mean operational efficiency of 73.92%, representing an efficiency gain compared to case 2a over a 48h time horizon. The total microgrid operating cost is $1233.7 for the same period. This slight improvement in efficiency is achieved by adjusting the operating point of the electrolyzer and optimally selecting the temperature and pressure at each instance, based on the behavior illustrated in Fig. 4.

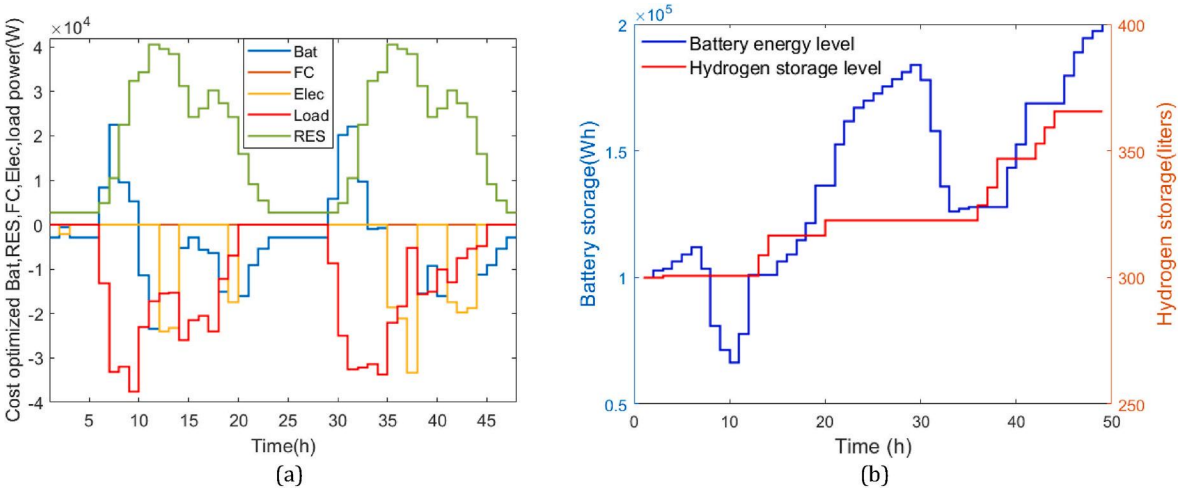

Fig. 7. Cost optimized EMS (a) optimal power schedule (b) battery and hydrogen storage profiles.

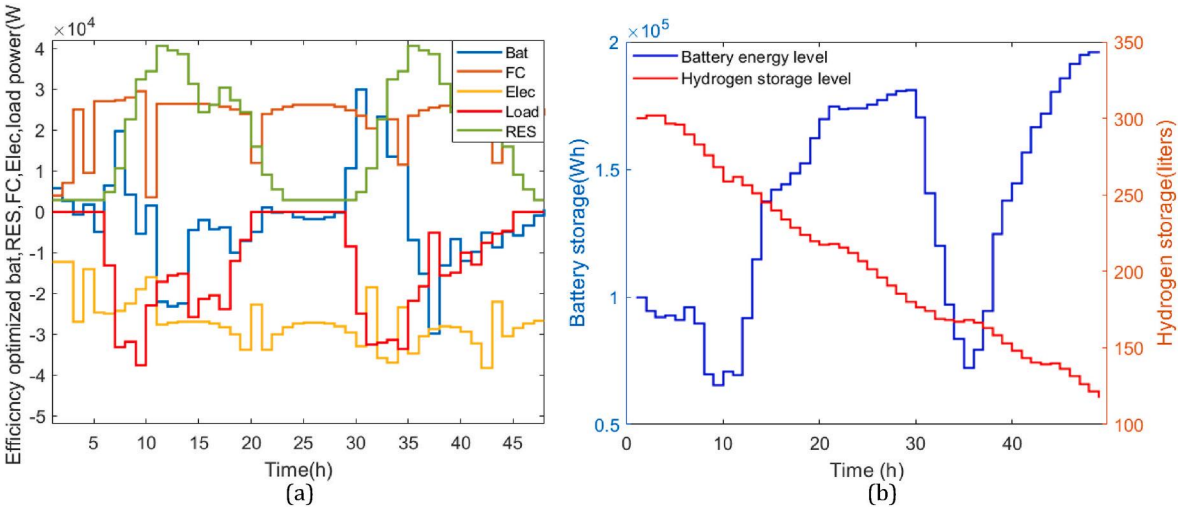

Fig. 8. Electrolyzer efficiency-based EMS (a) optimal power schedule (b) battery and hydrogen storage profiles.

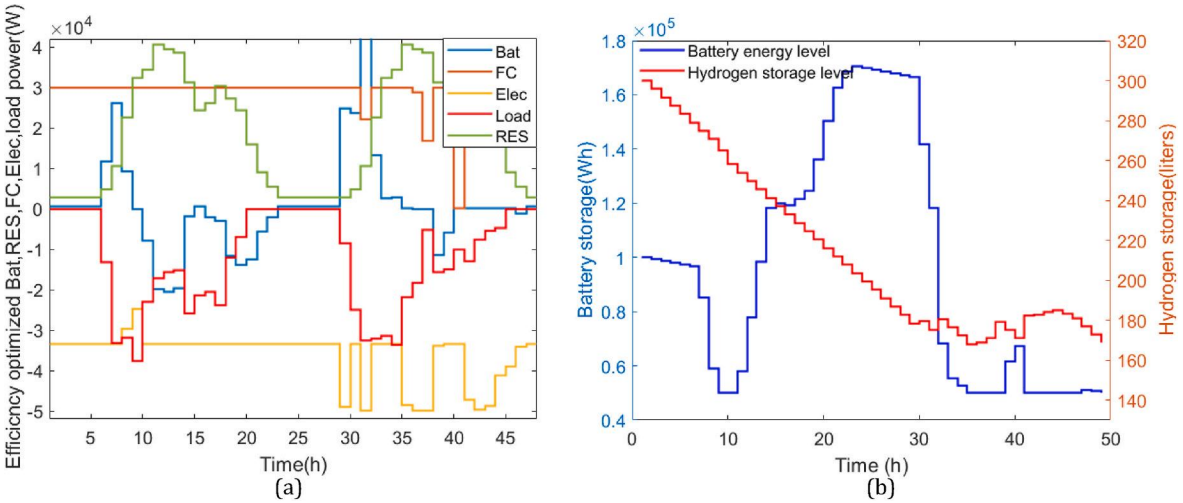

Fig. 9. TPO electrolyzer efficiency-based EMS (a) optimal power schedule (b) battery and hydrogen storage profiles.

6.4. Case 3a: Multi-objective optimization considering cost and electrolyzer efficiency

The total objective of the DC microgrid system combines both the operational cost and the electrolyzer efficiency objectives. As shown in (33), it is formulated as a normalized objective function using a weighted sum approach. The red curve in Fig. 12 presents the Pareto front of the scheme, illustrating the variation of the cost and efficiency objectives with the applied weight. For example, the final point on the curve corresponds to a weight of 0.1 on the cost objective and 0.9 on the efficiency objective. It is evident that assigning a higher weight to the cost objective enables the EMS to achieve lower operational costs at the expense of reduced hydrogen production, and vice versa. In an ideal scenario, the optimal operating point would simultaneously achieve both minimum operational cost and maximum efficiency. To identify this point, the Euclidean distance from each simulated point on the Pareto front to the ideal point is calculated. The point with the minimum distance is then selected as the optimal operating point.

Fig. 10a and Fig. 10b represent the results associated with this selected optimal point. Compared to Case 2, electrolyzer operation is significantly reduced due to the inclusion of the cost objective in the normalized objective function. Furthermore, the fuel cell operates at a significantly lower level, and even the usage of the battery system is reduced. Both the hydrogen and battery storage systems tend to store energy while maintaining the power balance of the microgrid. In this simulation, the electrolyzer system achieves a mean operational efficiency of 65.94% with a total cost for the microgrid operation of $202.9. These results highlight the balanced performance of the multi-objective-based scheme compared to the cost-only and efficiency-only schemes.

6.5. Case 3b: Temperature and Pressure Optimized Multi-Objective (TPO-MO) operation

In this section, the operating temperature and pressure, along with the current density, are optimized within predefined ranges, as described in Section 5.4. The operating temperature is allowed to vary between 310 K and 360 K, while the operating pressure can range from 1 bar to 20 bar. The optimization framework simultaneously minimizes the operating cost and maximizes the electrolyzer system efficiency, considering the hourly variation in the electrolyzer's operating power. In this multi-objective scenario, the EMS converges the temperature to approximately 360 K, while the pressure again dynamically varies between 9 bar and 11 bar. The blue curve in Fig. 12 represents the Pareto front of the scheme, from which the optimal operating point for the microgrid is selected. Fig. 11a and b represent the optimal power profiles and storage variation results corresponding to the selected optimal points. Compared to case 3a, the electrolyzer operates more frequently. The average operating power for electrolyzers and fuel cells has increased from 4.16 kW to 0.08 kW to 4.83 kW and 0.73 kW, respectively. The main reason for this increase is the allowance of operating temperature and operating pressure to vary within the selected region. TPO enables the electrolyzer systems to operate at slightly higher efficiency, which improves the efficiency-related term in the normalized objective function. This shifts the normalized objective slightly and changes the optimal operating point of the microgrid. In this case, the electrolyzer system achieves a mean operational efficiency of 68.79%, with an efficiency gain of 2.85% compared to case 3a. The total cost for microgrid operation is $207.5 over 48h.

6.6. Significance of multi-objective case studies

Fig. 12 presents a comparison between the Pareto fronts of the multi-objective EMS and the TPO-based multi-objective EMS. The figure clearly shows that the multi-objective EMS consistently achieves lower operational costs across all dynamic weight settings. As the weight is assigned to the cost objective increases, the cost increment of the multi-objective EMS relative to the TPO-based EMS also increases. With applied weights of 0.1, 0.5, and 0.9, the cost difference percentages are 3.2%, 2.6%, and 3.8%, respectively. When the efficiency objective is assigned the lowest dynamic weight of 0.1, the multi-objective EMS still demonstrates strong performance. It achieves nearly a 68% reduction in the efficiency objective value compared to the TPO-based multi-objective EMS. However, this efficiency difference significantly decreases to approximately 4.2% at the optimal operating point (weight of 0.5), and further reduces to around 2.6% at a weight of 0.9. This demonstrates the superior performance of the proposed EMS in terms of the efficiency objective at lower dynamic weights, with only a marginal increase in cost. This improvement is directly related to the introduction of the variable efficiency behavior of the electrolyzer system, as illustrated in Figs. 3 and 4. When the weight applied to the efficiency objective is low, the multi-objective EMS is unable to sufficiently shift the electrolyzer's operating point toward the higher-efficiency region shown in Fig. 3. In contrast, even at the lowest applied weight, the TPO-based multi objective EMS can shift the operating point further along the efficiency curve. As the applied weight increases, both EMS strategies can shift the operating point further along the efficiency curve, thereby achieving higher efficiencies. Even with higher weight coefficients, the TPO-based multi-objective EMS continues to outperform the conventional multi-objective case. It achieves a higher efficiency objective by selecting the optimal operating point along the efficiency curve illustrated in Fig. 3.

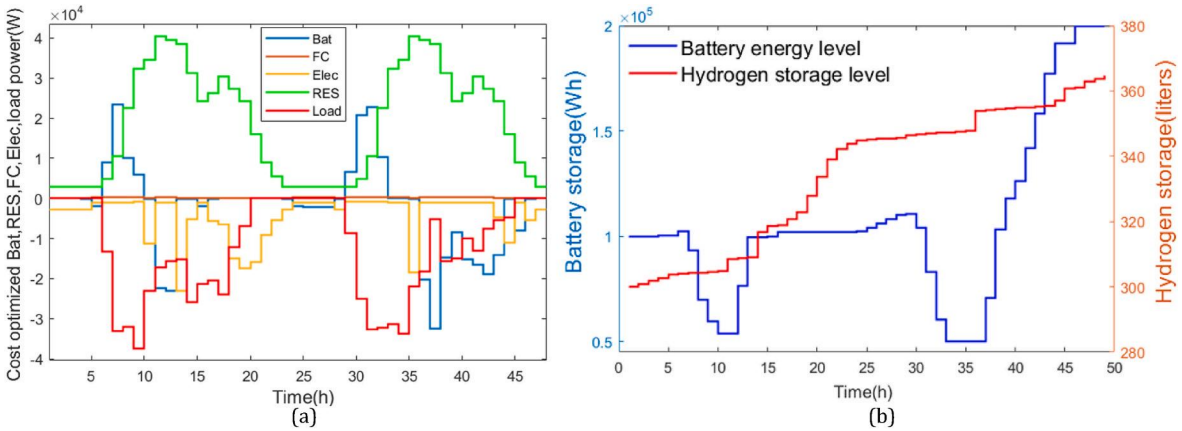

Fig. 10. Multi objective-based EMS (a) optimal power schedule (b) battery and hydrogen storage profiles.

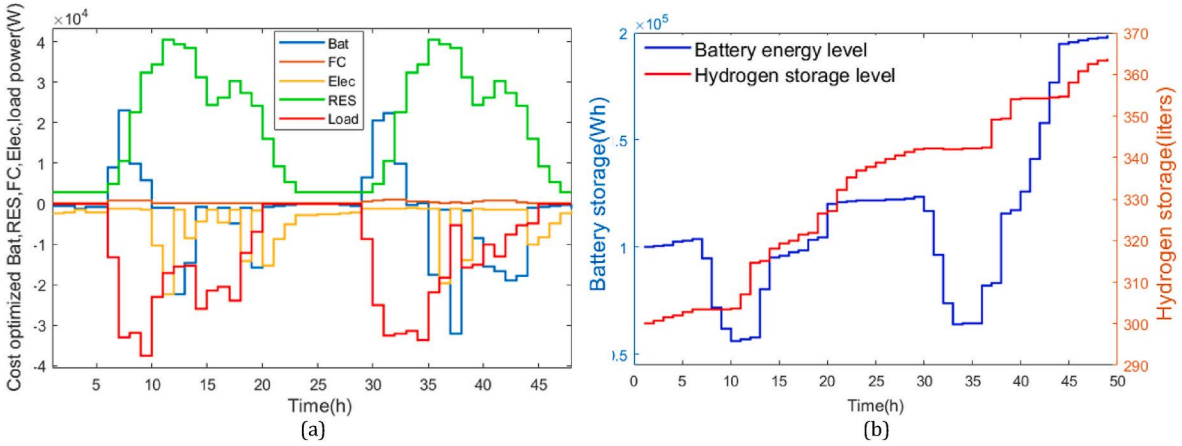

Fig. 11. TPO-MO EMS (a) optimal power schedule (b) battery and hydrogen storage profiles.

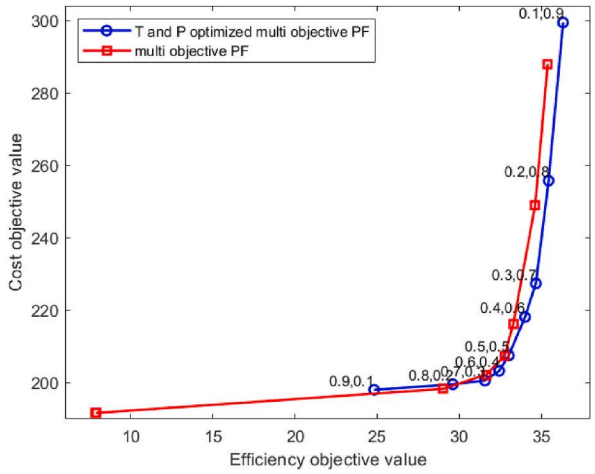

Fig. 12. Comparison of Pareto fronts.

7. Comparison and validation

The proposed novel objective formulation enables the microgrid to operate while satisfying all required constraints, as demonstrated in the previous sections. A direct comparison of the proposed strategy with recent related works is not carried out for several reasons, as discussed below. First, there are limited studies closely related to the present work, and for the available ones, most of the necessary data are not publicly accessible. Moreover, since this study primarily focuses on the PEM electrolyzer system, comprehensive manufacturing and performance data of the electrolyzer are required for accurate modeling, which are not available in the referenced studies. In some cases, system configurations and sizing parameters are also incompatible. Therefore, instead of a numerical comparison, this study qualitatively positions its contributions by highlighting methodological advancements and operational improvements relative to the recent literature. Table 4 presents the combinations of energy sources and storage technologies, along with a brief discussion of the limitations of recent studies.

Furthermore, in this study, the proposed EMS is evaluated using available renewable generation and load profiles to focus on the impact of integrating temperature-pressure dependent PEM electrolyzer system modelling within the optimization framework. Although advanced data-driven forecasting methods such as Long Short-Term Memory (LSTM) could be used to generate predictions for PV/wind/wave generation and load demand, forecasting is not considered in the present work. Incorporating forecasting and assessing the influences within the scheduling framework will be explored in future research to further support practical real-time deployment.

To validate its performance, the proposed strategy is compared against four EMS strategies applied to the same DC microgrid. Two conventional rule-based strategies are introduced: one prioritizes battery operation, while the other prioritizes electrolyzer and fuel cell operation. Evaluating both cases enables a comparison between low-cost operation and high-efficiency electrolyzer operation, as discussed in Section 6. In addition, a metaheuristic-based EMS using the Particle Swarm Optimization (PSO) algorithm is developed for comparison. The proposed formulation for electrolyzer system efficiency is nonlinear and involves a high-dimensional, large-scale search space for battery, electrolyzer, fuel cell power outputs, and electrolyzer operating temperature and operating pressure. PSO is selected for this comparison due to its ability to effectively handle nonlinearities, perform large-scale search, and balance exploration and exploitation in the optimization process. Operation cost, electrolyzer mean efficiency, and percentage cost-saving values are compared across three case studies: cost-based EMS, efficiency-based EMS, and multi-objective-based EMS. Furthermore for the MINLP approach, convergence curves were generated from the successive objective function values recorded during the branch-and-bound iterations of the BMIBNB solver in YALMIP, allowing consistent comparison with the PSO algorithm.

7.1. Cost-based EMS

Since cost is introduced as the sole objective, heuristic methods tend to suppress the operation of hydrogen components. Table 5 illustrates the cost and percentage cost-saving values. The results show that the EMS strategy formulated as a MINLP problem and solved using the BMIBNB solver achieves the lowest operational cost among the four strategies. The percentage cost reduction achieved ranges from 36.53% to 0.04%. Traditional strategy 2, which prioritizes electrolyzer and fuel cell operation, results in the highest operational cost. Strategy 1, which focuses on battery prioritization, also fails to reach an optimal point due to its rule-based nature. Compared to the PSO approach, the MINLP-based EMS achieves nearly equivalent performance, with only a 0.39% cost difference. Fig. 13a illustrates the hydrogen storage utilization for all four methods. Since cost is selected as the optimization objective, the battery is preferred as the lower-cost energy storage option compared to hydrogen. Consequently, all three optimization-based methods exhibit similar behavior, with only minor deviations related to solver characteristics. Fig. 13b illustrates the convergence curves for the PSO and MINLP strategies. Although deterministic MINLP solvers do not typically generate heuristic-style convergence curves, the plot here represents the evolution of the objective function value across successive branch-and-bound iterations within the BMIBNB process. This allows a

Table 4
Comparison of the proposed study.

Ref	Microgrid	EMS/Control	Discussion
[18]	PV, Bat, Elec, HS, FC	Decentralized with mode-triggered droop control	Operates in eight predefined EMS modes of the microgrid, which lack the flexibility to adapt to variable loads and renewable energy conditions. No formulation integrating hydrogen system dynamics. Hydrogen subsystem is included at the EMS level, but operation is mode-driven, and efficiency-optimal operation is not considered.
[19]	PV, Bat, Elec, HS, FC	Rule-based with PSO-based sizing	Electrolyzer and fuel cell performance are modeled in a simplified manner. The electrolyzer operating pressure is constrained by the tank limit, not making the operating environment an optimization decision. The EMS objective neglects the efficiency of the hydrogen system where focus is primarily on optimal sizing.
[20]	PV, wind, grid, Bat, Elec, HS, FC,	Hierarchical control with MPC	Practical MPC deployment raises scale issues, and the work is tied to a specific experimental platform and assumptions about emulated renewables and V2G behaviour. Optimization is limited to restricting the switching of the hydrogen components only. Hydrogen consumption and the nonlinear behavior of electrolyzer efficiency are ignored in the objective formulations.
[12]	PV, Wind, Hydro, Bat, Elec, HS, FC	Rule-based with demand response	DR + PLC supervisory logic sends excess energy to the electrolyzer and use FC when RES is insufficient, not optimizing electrolyzer operating efficiency -inside the EMS objective. Incorporates DR and hydrogen storage to reduce costs, but excludes efficiency-based optimization and detailed electrolyzer modeling.
[21]	PV, SC Elec, HS, FC	Frequency-splitting power allocation	Focuses on power allocation between hydrogen and electric systems. It doesn't cover multiple RES offshore variability and long-horizon economic dispatch. Focuses on power allocation with outer H_2 flow optimization and inner allocation, without integrating electrolyzer efficiency as a nonlinear function of T-P-I within a cost-efficiency EMS.
[22]	PV, Bat, SC, FC	Metaheuristic PSO	The equivalent consumption minimization method is formulated only for fuel cells, batteries, and supercapacitor systems. Electrolyzer dynamics and efficiency are not represented. With a simplified load setting and a single RES, it may not reflect highly variable offshore load and multiple RES uncertainty.
[23]	Wind, Bat, Elec, HS, FC	Distributionally robust chance constrained	This study works strongly on uncertainty issues. Considers nonlinear electrolyzer efficiency but assumes a constant operating environment. It lacks temperature- and pressure-dependent optimization.
[24]	Grid, DG, Bat, Elec, HS, FC	Two-stage scheduling	Two-stage (day-ahead with MIPL + real-time with MIQP-MPC) scheduling, with piecewise linear approximations of hydrogen device models, is developed. However, objectives include only general cost terms and ignore hydrogen system efficiency and degradation.
[25]	PV, Wind, Wave, Bat, Elec, HS, FC	DC link voltage control	DC-link-based voltage control maintains microgrid stability. But it excludes cost considerations and formulations of hydrogen system efficiency since detailed economic analysis is not considered.
This Study	PV, Wind, Wave, Bat, Elec, HS, FC	Hierarchical MINLP-based	A novel objective formulation is developed by dynamically integrating electrolyzer system efficiency as a function of current, temperature, and pressure. A multi-objective EMS optimizes both cost and hydrogen system efficiency. The model captures the nonlinear T-P-I behavior of the electrolyzer and evaluates its impact on microgrid performance under offshore renewable conditions.

direct comparison of convergence trends between the two methods. It clearly demonstrates the superiority of the MINLP method, which achieves the optimal solution within just three iterations.

7.2. Efficiency-based EMS

To evaluate the effectiveness of the proposed efficiency-based formulation, this study applies MINLP and PSO-based EMS strategies across two scenarios: an efficiency-optimized EMS and a TPO-based efficiency-optimized EMS. Table 6 presents the mean efficiency of the electrolyzer system, associated costs, and the percentage cost gain. The results indicate the effectiveness of the developed EMS strategy using MINLP, which operates with a higher electrolyzer mean efficiency compared to PSO under both general and temperature and pressure optimized conditions. Optimizing pressure and temperature enables the electrolyzer system to operate at a slightly higher efficiency, thereby increasing the efficiency component of the normalized objective function. Under optimized conditions, the MINLP-based EMS scheme achieves a 1.7% increase in efficiency. Since the objective function is formulated solely on electrolyzer system efficiency, operating the electrolyzer at higher power levels positively influences optimal system performance, resulting in higher mean efficiency. However, when considering operational costs, the MINLP-based strategy incurs a 25.1% increase in cost under optimized conditions compared to general operation, due to the higher utilization of the electrolyzer. However, under both general and optimized conditions, the proposed MINLP-based strategy achieves 0.3% and 0.1% improvements over the PSO-based strategy, demonstrating the superiority of the proposed scheme.

Table 5
Cost-based EMS stats.

EMS type	Cost ($)	% Cost saving	Computational time
Traditional 1	191.78	−0.04 %	0.729 s
Traditional 2	260.71	−36.53 %	0.793 s
PSO	192.45	−0.39 %	178.5 s
MINLP	191.69	-	21.96 s

In terms of hydrogen storage utilization, both PSO and MINLP-based strategies demonstrate dynamic hydrogen capture capability, utilizing the storage more consistently throughout the operation. When comparing the EMS strategies individually, PSO tends to use the electrolyzer more frequently, whereas MINLP relies more on fuel cell operation. Fig. 14a illustrates the hydrogen storage level variation over time for each of the four scenarios. Compared to PSO, MINLP tends to use fuel cells more frequently, leading to lower hydrogen levels. Notably, under temperature- and pressure-optimized conditions, both PSO and MINLP curves tend to shift downward relative to general operation. Due to variations in temperature and pressure, the objective function shifts, leading to increased electrolyzer operation, which in turn elevates fuel cell usage. However, since the heating value of hydrogen (used for electrolyzer hydrogen generation calculations) is higher than its energy density (used for fuel cell hydrogen consumption calculations), the hydrogen storage level decreases over time. Fig. 15a illustrates the convergence curves for the efficiency-based EMS under both general and optimized operating conditions. As before, MINLP plot represents the evolution of the objective function value across successive branch-and-bound iterations within the BMIBNB process. The results indicate that the MINLP method achieves the optimal solution within the first few iterations for both cases. In contrast, the PSO method fails to reach the same solution and requires more than 200 iterations in both scenarios. Furthermore, both strategies require additional iterations to achieve the optimal solution under temperature- and pressure-optimized operations due to the more complex formulations and the tighter, increased number of constraints involved.

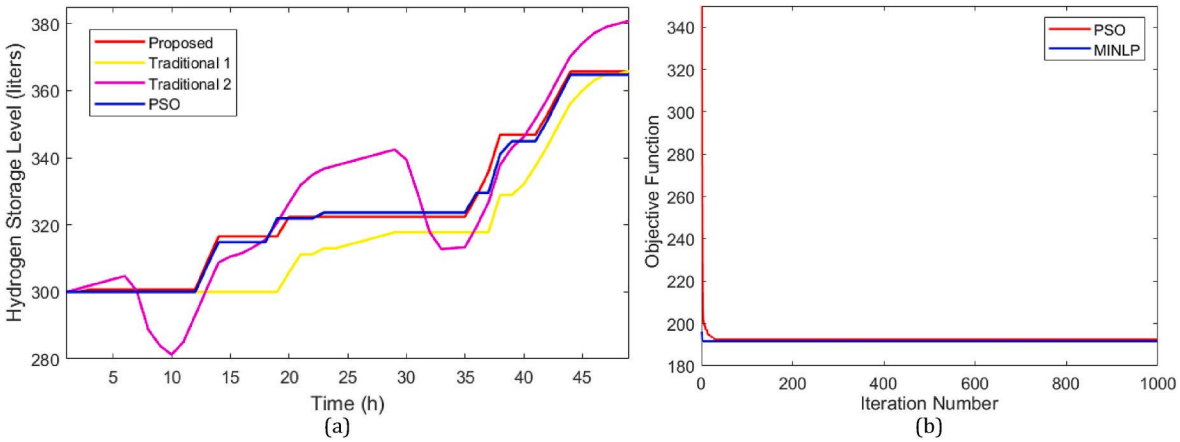

Fig. 13. Cost-based EMS (a) hydrogen storage utilization (b) Solver convergence curves.

Table 6
Efficiency-based EMS stats.

EMS type		Mean Efficiency (%)	Effi gain	Cost ($)	Cost Gain (%)
General	PSO	71.9	-	992.4	-
	MINLP	72.2	-	986.1	-
T and P opt	PSO	73.8	1.9	1021.2	+2.9
	MINLP	73.9	1.7	1233.7	+25.1

7.3. Multi-objective-based EMS

This section validates the proposed multi-objective-based objective formulation through the implementation of MINLP and PSO-based EMS strategies across two distinct scenarios: a general multi-objective EMS and a TPO-based multi-objective EMS. The results indicate that the developed MINLP-based EMS strategy achieves the highest electrolyzer system mean efficiency, compared to the PSO-based scheme under both general and optimized conditions. However, the mean efficiency is reduced by 6.8% and 5.1% under general and temperature- and pressure-optimized conditions, respectively, compared to the efficiency-based scheme. Since both efficiency and cost are included in the objective function, the optimal point is influenced by both factors, allowing a balanced trade-off between cost- and efficiency-based schemes. This balance is further evident in the cost results. The multi-objective-based scheme achieves a lower cost than the efficiency-based scheme but a higher cost than the cost-based scheme, providing a well-balanced operation between the two extremes. Furthermore, under both general and optimized conditions, the proposed MINLP-based strategy achieves notable efficiency gains of 6.9% and 7.4% compared to the PSO-based strategy, demonstrating the superiority of the proposed approach. In terms of cost, the MINLP-based strategy achieves significantly lower operating costs, by approximately 63% and 67%, relative to the PSO-based method. This improvement is likely due to the PSO algorithm converging to local optima, caused by the nonlinear and complex nature of the efficiency term in the objective function during the optimization process.

Fig. 14b illustrates the hydrogen storage level variation over time for each simulation. In this case, both the PSO and MINLP schemes tend to utilize only the electrolyzer, with zero operations of the fuel cell, which increases the hydrogen storage level. As in the previous efficiency-based EMS study, the TPO curves in both the PSO and MINLP schemes exhibit a downward shift for the same underlying factors. Fig. 15b illustrates the convergence curves for the multi-objective-based EMS under both general and optimized operating conditions. Consistent with previous results, the MINLP method achieves the optimal solution in significantly fewer iterations than PSO in both cases. However, compared to the previous two EMS strategies, even the MINLP approach requires more than 100 iterations due to the increased complexity of the multi-objective formulation. Compared to PSO, the optimal solutions obtained by MINLP show a notable improvement, demonstrating the superiority of the method. As before, the optimized-condition case requires more iterations to reach the optimal solution because of the tighter and increased number of constraints in the formulation (see Table 7).

Overall, the proposed EMS with dynamic modeling of electrolyzer efficiency provides a clear improvement over constant-efficiency assumptions. This strategy accounts for fluctuations in power, temperature, and pressure in the proposed DC microgrid. This is specifically

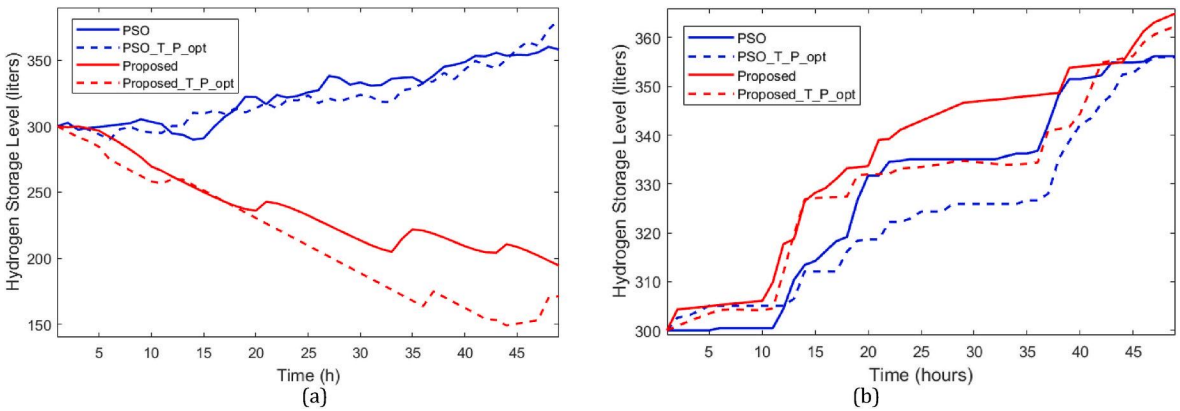

Fig. 14. Hydrogen storage utilization comparison with (a) efficiency-based EMS (b) multi-objective-based EMS.

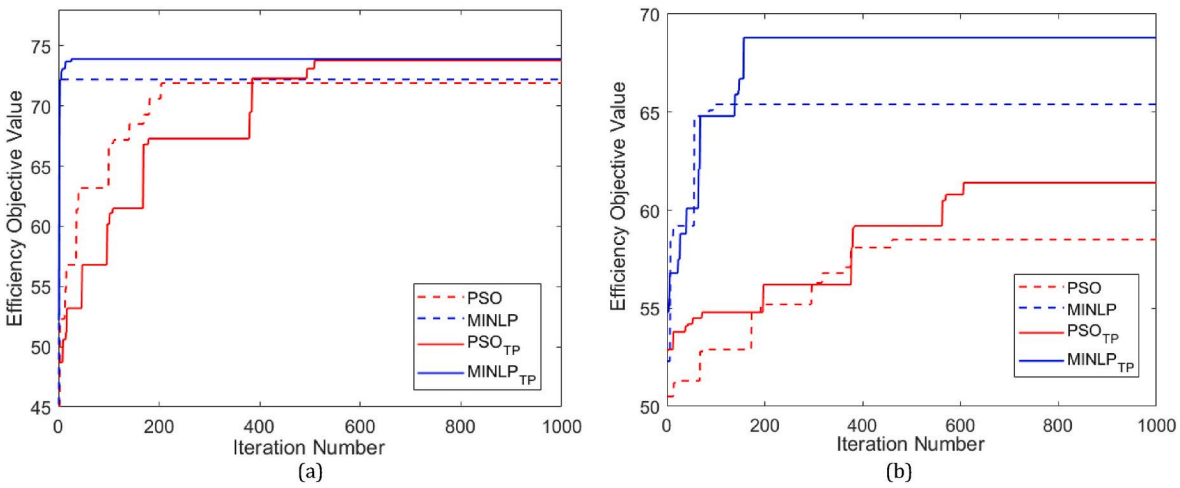

Fig. 15. Solver convergence curves (a) efficiency-based EMS (b) multi-objective-based EMS.

Table 7
Multi-objective-based EMS stats.

EMS type		Mean Efficiency (%)	Effi gain	Cost ($)	Cost Gain (%)
General	PSO	58.5	-	557.3	-
	MINLP	65.4	-	202.9	-
T and P opt	PSO	61.4	2.9	644.8	+15.7
	MINLP	68.8	3.1	207.5	+2.27

valuable for offshore conditions, where renewable generation is intermittent, storage is limited with space and weigh restrictions, and environmental conditions such as temperature, humidity, and salinity affect operation. By adjusting the electrolyzer's operating points, the system improves hydrogen efficiency, minimizes energy losses, and enhances reliability in islanded offshore conditions.

8. Conclusion and future studies

This paper proposes a novel objective function based on electrolyzer system efficiency to enable optimal utilization of hydrogen energy through coordinated control of the electrolyzer and fuel cell systems. Unlike most existing approaches, which assume constant electrolyzer efficiency within the EMS, the proposed formulation models the electrolyzer efficiency as a function of operating current, temperature, and pressure. The effectiveness of the proposed strategy was validated through multiple case studies. The developed DC microgrid operates under both efficiency-maximization and multi-objective optimization scenarios, incorporating Temperature- and pressure-optimized operation of the electrolyzer system. In the efficiency-maximization scenario, the electrolyzer system achieved a mean operational efficiency of 72.19% under constant conditions, which improved to 73.92% with optimized temperature and pressure. In the multi-objective EMS scenario, temperature- and pressure-optimized operation resulted in a mean efficiency of 68.8%, reflecting an improvement of 3.1% over constant operation. Additionally, the performance of the proposed MINLP-based EMS was compared with two widely used strategies: rule-based and PSO-based EMS. Under both constant and temperature- and pressure-optimized conditions, the MINLP-based EMS demonstrated improved mean efficiencies of 5.9% and 7.4% compared with the rule-based and PSO-based approaches, respectively. These findings highlight the effectiveness of the proposed objective function and optimization framework for islanded DC microgrids. The results demonstrate its capability to enhance hydrogen system efficiency while enabling operation strategies that balance cost and performance, thereby shifting system behavior toward more economical, hydrogen-optimized regimes.

In future work, the effectiveness of the proposed novel formulations, as well as the benefits of temperature and pressure-optimized operation of the electrolyzer system, can be evaluated through experimental validation. The developed microgrid EMS can be further evaluated in a real-world offshore environment, which would demonstrate both its capability for seamless integration and its scalability for larger, complex, and hybrid systems. Furthermore, the proposed strategy can be extended to incorporate the degradation behavior of the PEM electrolyzer. Since degradation-related parameters, such as current density, temperature, pressure, and membrane operation, are already included in the developed formulations, integrating degradation analysis into the system is expected to be straightforward. Although robustness under uncertainty is not discussed in this study, it is recognized that uncertainties play a significant role in hydrogen–renewable microgrids. These uncertainties arise from renewable generation variability, hydrogen system characteristics (electrolyzer efficiency, electrolyzer and fuel cell degradations, pressure–temperature variations), and forecasting errors in load demand. Integrating such uncertain factors would provide deeper insights into the resilience of the proposed EMS. Additionally, a comprehensive mathematical framework can be developed to accurately identify the optimal operating point along the Pareto front within the multi-objective optimization strategy.

CRediT authorship contribution statement

Bawantha Indrajith: Writing – review & editing, Writing – original draft, Visualization, Validation, Software, Methodology, Investigation, Formal analysis, Conceptualization. **Kosala Gunawardane:** Writing – review & editing, Visualization, Supervision, Resources, Project administration, Funding acquisition, Formal analysis. **Md Alamgir Hossain:** Writing – review & editing, Supervision, Resources, Investigation, Formal analysis. **Li Li:** Writing – review & editing, Supervision, Software, Resources, Formal analysis. **Robert Nicholson:** Writing – review & editing, Supervision, Formal analysis. **Ramon Zamora:** Writing – review & editing, Supervision, Project administration, Funding acquisition, Formal analysis. **Mark Anthony Preece:** Writing – review & editing, Project administration, Formal analysis.

Declaration of competing interest

The authors declare that they have no known competing financial interests or personal relationships that could have appeared to influence the work reported in this paper.

Acknowledgements

The authors acknowledge the financial support of the Blue Economy Cooperative Research Centre, established and supported under the Australian Government's Cooperative Research Centers Program, grant number CRC-20180101.

The authors acknowledge The New Zealand King Salmon Company Ltd for providing the data that supported this research study.

References

[1] Global overview – renewables 2024 – analysis," IEA. Accessed: May 2, 2025. [Online]. Available: https://www.iea.org/reports/renewables-2024/global-overview.
[2] Global hydrogen review 2024 – analysis," IEA. Accessed: January. 10, 2025. [Online]. Available: https://www.iea.org/reports/global-hydrogen-review-2024.
[3] Rostirolla G, et al. A survey of challenges and solutions for the integration of renewable energy in datacenters. Renew Sustain Energy Rev Mar. 2022;155:111787. https://doi.org/10.1016/j.rser.2021.111787.
[4] Uddin M, Mo H, Dong D, Elsawah S, Zhu J, Guerrero JM. Microgrids: a review, outstanding issues and future trends. Energy Strategy Rev Sept. 2023;49:101127. https://doi.org/10.1016/j.esr.2023.101127.
[5] Raya-Armenta JM, Bazmohammadi N, Avina-Cervantes JG, Sáez D, Vasquez JC, Guerrero JM. Energy management system optimization in islanded microgrids: an overview and future trends. Renew Sustain Energy Rev Oct. 2021;149:111327. https://doi.org/10.1016/j.rser.2021.111327.
[6] Al-Ismail FS. DC microgrid planning, operation, and control: a comprehensive review. IEEE Access 2021;9:36154–72. https://doi.org/10.1109/ACCESS.2021.3062840.
[7] Anderson AA, Suryanarayanan S. Review of energy management and planning of islanded microgrids. CSEE J Power Energy Syst June 2020;6(2):329–43. https://doi.org/10.17775/CSEEJPES.2019.01080.
[8] Choudhury S. Review of energy storage system technologies integration to microgrid: types, control strategies, issues, and future prospects. J Energy Storage Apr. 2022;48:103966. https://doi.org/10.1016/j.est.2022.103966.
[9] Sharma P, Dutt Mathur H, Mishra P, Bansal RC. A critical and comparative review of energy management strategies for microgrids. Appl Energy Dec. 2022;327:120028. https://doi.org/10.1016/j.apenergy.2022.120028.
[10] Lauinger D, Caliandro P, Van herle J, Kuhn D. A linear programming approach to the optimization of residential energy systems. J Energy Storage Aug. 2016;7:24–37. https://doi.org/10.1016/j.est.2016.04.009.
[11] Vitale F, Rispoli N, Sorrentino M, Rosen MA, Pianese C. On the use of dynamic programming for optimal energy management of grid-connected reversible solid oxide cell-based renewable microgrids. Energy June 2021;225:120304. https://doi.org/10.1016/j.energy.2021.120304.
[12] Maghami MR, Hassani R, Gomes C, Hizam H, Othman ML, Behmanesh M. Hybrid energy management with respect to a hydrogen energy system and demand response. Int J Hydrogen Energy Jan. 2020;45(3):1499–509. https://doi.org/10.1016/j.ijhydene.2019.10.223.
[13] Zehra SS, Ur Rahman A, Ahmad I. Fuzzy-barrier sliding mode control of electric-hydrogen hybrid energy storage system in DC microgrid: modelling, management and experimental investigation. Energy Jan. 2022;239:122260. https://doi.org/10.1016/j.energy.2021.122260.
[14] Vivas FJ, et al. Multi-objective fuzzy logic-based energy management system for microgrids with battery and hydrogen energy storage system. Electronics July 2020;9(7). https://doi.org/10.3390/electronics9071074.
[15] Akbari-Dibavar A, Sohrabi Tabar V, Ghassem Zadeh S, Nourollahi R. Two-stage robust energy management of a hybrid charging station integrated with the photovoltaic system. Int J Hydrogen Energy Apr. 2021;46(24):12701–14. https://doi.org/10.1016/j.ijhydene.2021.01.127.
[16] Nojavan S, Akbari-Dibavar A, Farahmand-Zahed A, Zare K. Risk-constrained scheduling of a CHP-based microgrid including hydrogen energy storage using robust optimization approach. Int J Hydrogen Energy Nov. 2020;45(56):32269–84. https://doi.org/10.1016/j.ijhydene.2020.08.227.
[17] Tabar VS, Jirdehi MA, Hemmati R. Energy management in microgrid based on the multi objective stochastic programming incorporating portable renewable energy resource as demand response option. Energy Jan. 2017;118:827–39. https://doi.org/10.1016/j.energy.2016.10.113.
[18] Han Y, Yang H, Li Q, Chen W, Zare F, Guerrero JM. Mode-triggered droop method for the decentralized energy management of an islanded hybrid PV/hydrogen/battery DC microgrid. Energy May 2020;199:117441. https://doi.org/10.1016/j.energy.2020.117441.
[19] Marocco P, Ferrero D, Lanzini A, Santarelli M. Optimal design of stand-alone solutions based on RES + hydrogen storage feeding off-grid communities. Energy Convers Manag June 2021;238:114147. https://doi.org/10.1016/j.enconman.2021.114147.
[20] Mendes PRC, Isorna LV, Bordons C, Normey-Rico JE. Energy management of an experimental microgrid coupled to a V2G system. J Power Sources Sept. 2016;327:702–13. https://doi.org/10.1016/j.jpowsour.2016.07.076.
[21] Tang Y, Xun Q, Liserre M, Yang H. Energy management of electric-hydrogen hybrid energy storage systems in photovoltaic microgrids. Int J Hydrogen Energy Aug. 2024;80:1–10. https://doi.org/10.1016/j.ijhydene.2024.07.017.
[22] Abu SM, et al. An effective optimization algorithm for hydrogen fuel cell-based hybrid energy system: a sustainable microgrid approach. Int J Hydrogen Energy Jan. 2025;98:1341–55. https://doi.org/10.1016/j.ijhydene.2024.12.176.
[23] Shen Y, Zhai J, Kang Z, Zhao B, Gao X, Li Z. Distributionally robust chance-constrained energy management for island DC microgrid with offshore wind power hydrogen production. Energy Feb. 2025;316:134570. https://doi.org/10.1016/j.energy.2025.134570.
[24] Xie X, Quan X, Wu Z, Zeng F, Miu H, Yuan X. Optimizing AC/DC microgrid scheduling with electro-hydrogen hybrid energy storage for low-carbon buildings. Int J Hydrogen Energy July 2025;143:716–27. https://doi.org/10.1016/j.ijhydene.2025.05.016.
[25] Hossain MA. Experimental validation of DC-link based voltage control framework for islanded hydrogen DC microgrids. Int J Hydrogen Energy Nov. 2025;189:152033. https://doi.org/10.1016/j.ijhydene.2025.152033.
[26] One minute solar data. https://reg.bom.gov.au/climate/reg/oneminsolar/. [Accessed 16 August 2024].
[27] Kaabeche A, Belhamel M, Ibtiouen R. Sizing optimization of grid-independent hybrid photovoltaic/wind power generation system. Energy Feb. 2011;36(2):1214–22. https://doi.org/10.1016/j.energy.2010.11.024.
[28] Tildesley P. Droughty hill wind readings - tasmanian Earth resources satellite station (1995 -2011). Feb. 2013. https://doi.org/10.4225/08/5126C64FBEAA1.
[29] Borowy BS, Salameh ZM. Optimum photovoltaic array size for a hybrid wind/PV system. IEEE Trans Energy Convers Sept. 1994;9(3):482–8. https://doi.org/10.1109/60.326466.
[30] Correa JM, Farret FA, Canha LN, Simoes MG. An electrochemical-based fuel-cell model suitable for electrical engineering automation approach. IEEE Trans Ind Electron Oct. 2004;51(5):1103–12. https://doi.org/10.1109/TIE.2004.834972.
[31] Thanapalan KKT, Williams JG, Liu GP, Rees D. Modelling of a PEM fuel cell system. IFAC Proc Jan. 2008;41(2):4636–41. https://doi.org/10.3182/20080706-5-KR-1001.00780.
[32] Sedghisigarchi K, Feliachi A. Dynamic and transient analysis of power distribution systems with fuel Cells-part I: fuel-cell dynamic model. IEEE Trans Energy Convers June 2004;19(2):423–8. https://doi.org/10.1109/TEC.2004.827039.
[33] Görgün H. Dynamic modelling of a proton exchange membrane (PEM) electrolyzer. Int J Hydrogen Energy Jan. 2006;31(1):29–38. https://doi.org/10.1016/j.ijhydene.2005.04.001.
[34] Marangio F, Santarelli M, Calì M. Theoretical model and experimental analysis of a high pressure PEM water electrolyser for hydrogen production. Int J Hydrogen Energy Feb. 2009;34(3):1143–58. https://doi.org/10.1016/j.ijhydene.2008.11.083.
[35] Usman MR. Hydrogen storage methods: review and current status. Renew Sustain Energy Rev Oct. 2022;167:112743. https://doi.org/10.1016/j.rser.2022.112743.
[36] Klopčič N, Esser K, Rauh JF, Sartory M, Trattner A. Modelling hydrogen storage and filling systems: a dynamic and customizable toolkit. Int J Hydrogen Energy Jan. 2024;49:1180–95. https://doi.org/10.1016/j.ijhydene.2023.08.036.
[37] Scheepers F, et al. Improving the efficiency of PEM electrolyzers through membrane-specific pressure optimization. Energies Jan. 2020;13(3). https://doi.org/10.3390/en13030612.
[38] Scheepers F, et al. Temperature optimization for improving polymer electrolyte membrane-water electrolysis system efficiency. Appl Energy Feb. 2021;283:116270. https://doi.org/10.1016/j.apenergy.2020.116270.
[39] Sayed-Ahmed H, Toldy ÁI, Santasalo-Aarnio A. Dynamic operation of proton exchange membrane electrolyzers—Critical review. Renew Sustain Energy Rev Jan. 2024;189:113883. https://doi.org/10.1016/j.rser.2023.113883.
[40] Program records | hydrogen program." Accessed: June 12, 2025. [Online]. Available: https://www.hydrogen.energy.gov/library/program-records#fuel-cells.
[41] 2025 incremental purchase cost methodology and results for clean vehicles".
[42] Huynh DC, Ho LD, Dunnigan MW. Generation cost optimization of an islanded microgrid system with distributed generators and renewable energy sources. In: 2021 IEEE 2nd international conference on smart technologies for power, energy and control (STPEC); Dec. 2021. p. 1–6. https://doi.org/10.1109/STPEC52385.2021.9718640.
[43] Huynh DC, Dunnigan MW. Power generation cost minimization of an islanded diesel/wind turbine/fuel cell microgrid system. In: 2021 5th international conference on electrical, electronics, communication, computer technologies and optimization techniques (ICEECCOT); Dec. 2021. p. 665–9. https://doi.org/10.1109/ICEECCOT52851.2021.9708038.
[44] Beyazıt MA, Taşcıkaraoğlu A, Catalão JPS. Cost optimization of a microgrid considering vehicle-to-grid technology and demand response. Sustain Energy Grids Netw Dec. 2022;32:100924. https://doi.org/10.1016/j.segan.2022.100924.
[45] Boaro M, Fuselli D, Angelis FD, Liu D, Wei Q, Piazza F. Adaptive dynamic programming algorithm for renewable energy scheduling and battery management. Cogn Comput June 2013;5(2):264–77. https://doi.org/10.1007/s12559-012-9191-y.

[46] Zhang H, Su S, Lin G, Chen J. Efficiency calculation and configuration design of a PEM electrolyzer system for hydrogen production. Int J Electrochem Sci Jan. 2012; 7(5):4143–57. https://doi.org/10.1016/S1452-3981(23)19527-7.
[47] Khajuria R, Yelisetti S, Lamba R, Kumar R. Optimal model parameter estimation and performance analysis of PEM electrolyzer using modified honey badger algorithm. Int J Hydrogen Energy Jan. 2024;49:238–59. https://doi.org/10.1016/j.ijhydene.2023.07.172.
[48] De Silva YSK, Middleton PH, Kolhe ML. Performance comparison of mono-polar and bi-polar configurations of alkaline electrolysis stack through 3-D modelling and experimental fabrication. Renew Energy Apr. 2020;149:760–72. https://doi.org/10.1016/j.renene.2019.12.087.
[49] Noor Azam AMI, et al. Parametric study and electrocatalyst of polymer Electrolyte membrane (PEM) electrolysis performance. Polymers Jan. 2023;15(3):560. https://doi.org/10.3390/polym15030560.
[50] YALMIP. https://yalmip.github.io/. [Accessed 11 November 2024].
[51] Lofberg J. YALMIP : a toolbox for modeling and optimization in MATLAB. In: 2004 IEEE international conference on robotics and automation (IEEE cat. No.04CH37508); Sept. 2004. p. 284–9. https://doi.org/10.1109/CACSD.2004.1393890.